

Needle Insertion and Radioactive Seed Implantation in Human Tissues: Simulation and Sensitivity Analysis¹

Ron Alterovitz and Ken Goldberg
IEOR & EECS Departments
UC Berkeley

Jean Pouliot, Richard Taschereau, and I-Chow Hsu
Department of Radiation Oncology
UC San Francisco

Abstract – To facilitate training and planning for medical procedures such as prostate brachytherapy, we are developing an interactive simulation of needle insertion and radioactive seed implantation in soft tissues. We describe a new 2D dynamic FEM model based on a reduced set of scalar parameters such as needle friction, sharpness, and velocity, where the mesh is updated to maintain element boundaries along the needle shaft and the effects of needle tip and frictional forces are simulated. The computational complexity of our model grows linearly with the number of elements in the mesh and achieves 24 frames per second for 1250 triangular elements on a 750MHz PC. We use the simulator to characterize the sensitivity of seed placement error to physician-controlled and biological parameters. Results indicate that seed placement error is highly sensitive to physician-controlled parameters such as needle position, sharpness, and friction, and less sensitive to patient-specific parameters such as tissue stiffness and compressibility.

I. INTRODUCTION

Human surgery is increasingly based on minimally invasive procedures that operate inside the body through narrow openings, reducing disturbance to healthy tissue, minimizing risk of infection, and speeding recovery. Fast and accurate computer simulations of these procedures can facilitate physician training and assist in pre-operative planning and optimization.

Permanent seed brachytherapy is a minimally invasive medical procedure that has rapidly gained popularity for treating prostate cancer due to the excellent long-term outcomes. During the procedure, physicians use needles to permanently implant seeds inside the prostate that irradiate surrounding tissue over several months. The radioactive dose delivered should minimize healthy tissue damage while maximizing the destruction of cancerous cells. The success of this procedure depends on the accurate placement of radioactive seeds within the prostate gland [7, 15].

Before the implant procedure, a dosimetric plan is prepared based on static imaging of the prostate and medical considerations. Methods for calculating optimal seed locations are available [16, 12, 23]. Achieving the desired seed placement in the patient is left to the physician. Multiple seeds and biodegradable spacers are loaded into needles that the physician inserts horizontally

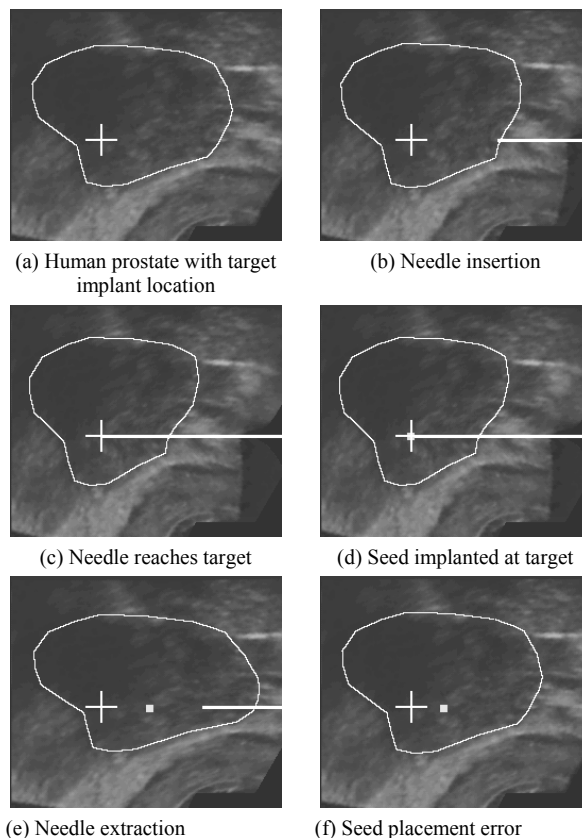


Fig. 1: Simulation of needle insertion based on an ultrasound image of a human prostate. Frame (a) outlines the prostate and displays the target implant location (white cross), which is fixed in the world frame. The simulated needle is inserted and places a radioactive seed (small square) at the target (d). After needle retraction, the *seed placement error*, the distance between the target and resulting seed location shown in (f), is 20% of the width of the prostate. Needle plans that compensate for tissue deformation can reduce placement errors like this that damage healthy tissue and fail to kill cancerous cells.

into the patient as shown in Fig. 2. Seeds and spacers are ejected from the needle when the depth specified by the dosimetric plan is reached.

Unfortunately, inserting and retracting needles causes the surrounding soft tissues to displace and deform: ignoring these deformations during the implantation results in misplaced seeds [15, 18], as demonstrated in Fig. 1. Although real-time ultrasound imaging is available during the procedure, it does not produce crisp tissue boundaries and cannot be used to precisely track the penetration of the needle into the deformed prostate. A dynamic simulation can facilitate procedure planning by

¹ IEEE International Conference on Robotics and Automation, Taipei, Taiwan, May 2003. For more information, please contact ron@ieor.berkeley.edu or goldberg@ieor.berkeley.edu or visit <http://alpha.ieor.berkeley.edu/ron/research>.

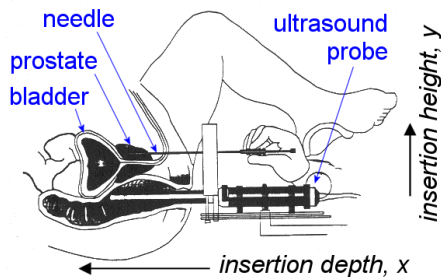


Fig. 2: During brachytherapy, needles carrying radioactive seeds are inserted transperineally into the patient, who is lying on his back [15].

allowing a physician or optimizing planner to determine how physician-controlled and patient-specific parameters will affect seed placement.

II. RELATED WORK

DiMaio and Salcudean performed pioneering work in simulating the deformations that occur during needle insertion [8]. Their simulation, based on a quasi-static finite element method, achieves extremely fast update rates (500Hz) and high accuracy (node displacement error of 1.4mm for needle penetration of 70mm). High accuracy requires a calibration phase where the force distribution along the needle shaft is estimated based on observed tissue deformations. This force distribution, which is modeled with a parameterized surface in Figure 11 of [8], may be difficult to measure in vivo.

We propose an alternative model based on a reduced set of scalar parameters such as needle friction, sharpness, and velocity. These parameters can be selected, within limits, by the physician to improve placement accuracy. This model allows us to produce an interactive simulation and analyze the sensitivity of current medical methods to these parameters.

Needle insertion simulation requires calculating deformations of soft tissue when forces are applied. The history of offline animation and real-time simulation of deformable objects is summarized in [10]. Mass-spring models have been common for simulating a diverse array of human tissues including muscles [20] and blood vessels [5]. These models are relatively easy to implement. However, they not only discretize the object into a set of finite point masses, they also discretize the equations of motion.

Unlike the mass-spring model, the finite element method (FEM) is based on the equations of continuum mechanics. The feasibility and potential of this approach for animation was demonstrated by Terzopolous [19]. Real-time visual performance for surgery simulation of the human liver using FEM was achieved by Stéphane Cotin et al. using a large preprocessing step [6]. They modeled tissue as a linearly elastic material and allowed only small quasi-static deformations.

The quasi-static assumption was relaxed by Zhuang [24] and Picinbono et al. [14], who simulated dynamic deformations of soft materials. Our needle insertion simulation includes this feature. Zhuang and Picinbono also simulate large deformations using quadratic strain, which generates a nonlinear system of differential equations. To achieve real-time visual performance for reasonably sized meshes, Zhuang uses two key approximations: mass lumping and a graded mesh. The loss of realism resulting from mass lumping is relatively low, as shown experimentally for soft tissues in [2].

To accurately model large deformations, it may also be necessary to take into account the nonlinear elasticity of some materials [3, 22]. In [3], a FEM model was created of the female breast to track the position of a tumor for a biopsy procedure. Because of the large deformations caused by the compression, a piece-wise linear function was used to approximate the nonlinear elasticity of the tissues. We do not believe the deformations caused by needle insertion are sufficiently large to justify the use of this method for our application.

Mesh modification when simulating scalpel cutting often produces elongated elements [13]. This may significantly slow the FEM solving process, as shown in [9], and also may occur when simulating needle insertion. Nienhuys proposes an algorithm where most severely elongated elements in 3D are removed in a post-processing step that generally increases the number of elements by only 1% [13].

III. PROSTATE MODEL

A 2D slice of the prostate and surrounding tissues is defined using a mesh of triangular elements. This *reference mesh* G defines the geometry of the tissues, with each node's coordinate stored in the position vector \mathbf{x} . Applied forces displace each node by its corresponding entry in the displacement vector \mathbf{u} . The *deformed mesh* G' is constructed using the node coordinates $\mathbf{x} + \mathbf{u}$ in the world frame. For visualization, mesh G is used to obtain texture map coordinates for G' .

In this paper, we approximate soft tissues as linearly elastic homogeneous materials. The Young's modulus and Poisson ratio are set using the results of [11]. Additional tissue properties must be estimated, including the force required to cut a unit length of tissue, the force required to break membranes, and the static and kinetic coefficients or friction.

IV. COMPUTING SOFT TISSUE DEFORMATIONS

We use the finite element method (FEM) to compute the deformations of soft tissues when forces are applied by the needle. Rather than calculating only static deformations, we simulate the dynamic behavior of soft tissues by solving for the acceleration, velocity, and

displacement of each node for every time step to produce a history-dependant simulation.

A. FEM Formulation

The soft tissue is defined by a mesh composed of m discrete 3-node triangular elements created using n total nodes, each with 2 degrees of freedom. The FEM problem is defined by a system of $d=2n$ linear differential equations:

$$\mathbf{M} \mathbf{a}_i + \mathbf{C} \mathbf{v}_i + \mathbf{K} \mathbf{u}_i = \mathbf{f}_i \quad (1)$$

where \mathbf{M} is the mass matrix, \mathbf{C} is the damping matrix, \mathbf{K} is the stiffness matrix, \mathbf{f}_i is the external force vector, \mathbf{a}_i is the nodal acceleration vector, \mathbf{v}_i is the nodal velocity vector, and \mathbf{u}_i is the nodal displacement vector at time step i [25].

The vector \mathbf{f}_i represents the forces exerted by the needle on the tissue, as described in section V. The matrices \mathbf{M} , \mathbf{C} , and \mathbf{K} are properties of the material being modeled and are constructed by superimposing the element mass, damping, and stiffness matrices [25]. Hence, the number of non-zero entries in each of these matrices is $O(d)$. When a node is moved or constrained, these matrices must be updated, a process that takes constant time for each DOF. The time integration techniques described below are used to solve for \mathbf{a}_i , \mathbf{v}_i , and \mathbf{u}_i for each time step i .

B. Algorithms to Solve the FEM System

To integrate the differential system (1) over time, we use the Newmark method [21], which translates the differential system into a linear system of equations. The method includes parameters β and γ that determine the properties of the resulting linear systems. Let h be the time step duration. Displacement and velocity for the next time step are approximated as:

$$\begin{aligned} \mathbf{u}_{i+1} &= \mathbf{u}_i + h \mathbf{v}_i + (1-\beta) (h^2/2) \mathbf{a}_i + \beta (h^2/2) \mathbf{a}_{i+1} \\ \mathbf{v}_{i+1} &= \mathbf{v}_i + (1-\gamma) h \mathbf{a}_i + \gamma h \mathbf{a}_{i+1} \end{aligned}$$

For our application, we implement two solvers: a slow accurate solver for planning and a faster solver for interactive simulation. When real-time interactive performance is required as defined in section VI, the value of h is adaptive; it is set using the system clock to the amount of time that has passed since the last iteration was completed.

For accurate planning, we set the Newmark method parameters $\beta=0.5$ and $\gamma=0.5$ to obtain the implicit system:

$$\begin{aligned} (\mathbf{M} + h \mathbf{C}/2 + h^2 \mathbf{K}/4) \mathbf{a}_{i+1} &= \\ \mathbf{f}_{i+1} - (h \mathbf{C}/2 + h^2 \mathbf{K}/4) \mathbf{a}_i - (\mathbf{C} + h \mathbf{K}) \mathbf{v}_i - \mathbf{K} \mathbf{u}_i \\ \mathbf{v}_{i+1} &= \mathbf{v}_i + (1/2) h (\mathbf{a}_i + \mathbf{a}_{i+1}) \\ \mathbf{u}_{i+1} &= \mathbf{u}_i + h \mathbf{v}_{i+1} + (1/4) h^2 (\mathbf{a}_i + \mathbf{a}_{i+1}) \end{aligned}$$

Acceleration is obtained by solving the linear system using an iterative numerical method such as Gauss-Seidel or Conjugate Gradient that takes advantage of the sparsity of the matrices. Since \mathbf{K} , \mathbf{M} , and \mathbf{C} contain only $O(d)$ non-zero entries, the iterative method will take $O(d^2)$ time in the worst case, although typically the number of iterations is much less than d .

For interactive simulation, we avoid solving a linear system by setting the Newmark method parameters to $\beta=0$ and $\gamma=0.5$ to obtain the explicit system:

$$\begin{aligned} \mathbf{u}_{i+1} &= \mathbf{u}_i + h \mathbf{v}_i + (1/2) h^2 \mathbf{a}_i \\ (\mathbf{M} + h \mathbf{C}/2) \mathbf{a}_{i+1} &= \mathbf{f}_{i+1} - \mathbf{K} \mathbf{u}_{i+1} - \mathbf{C} (\mathbf{v}_i + h \mathbf{a}_i/2) \\ \mathbf{v}_{i+1} &= \mathbf{v}_i + (1/2) h (\mathbf{a}_i + \mathbf{a}_{i+1}) \end{aligned}$$

Mass lumping, which approximates the continuous material as a particle system, decouples the system of equations into a set of algebraic equations [24, 14]. Mass lumping results in a small loss of accuracy in the dynamics and material properties of the object, as shown experimentally in [2]. With mass lumping, each time step requires only $O(d)$ time to compute and does not require any extensive pre-computation.

In most cases, explicit integration is considered inferior to implicit integration because it is unstable for large time steps [4]. However, this instability is most prevalent for stiff materials since the maximum time step length is inversely proportional to the natural frequency of the dynamic system (1). Since the natural frequency is very small for soft tissues, explicit integration can be used effectively for these simulations [24].

V. SIMULATING NEEDLE PROCEDURES

Based on the brachytherapy procedure shown in Fig. 2, the physician selects a height and begins to insert the needle into the patient. Once the needle is in contact with tissue, we assume the needle's y-coordinate is fixed and it only moves parallel to the horizontal x-axis. We also assume that the needle is thin and rigid. In our simulation, the physician first selects a height and then can insert (move left) or retract (move right) the simulated needle at any realistic velocity and implant a seed at any time.

Rather than modeling the needle as a distinct meshed object, we instead simulate the forces applied by the needle to the soft tissue. This method for representing the needle facilitates real-time interactive performance since no expensive collision detection is required. The needle exerts force on the tissue at the needle tip, where the needle is displacing and cutting the tissue, and frictional forces are applied along the needle shaft [17]. Puncturing tissue membranes requires additional force at the needle tip. These forces applied by the needle are computed and the FEM force vector \mathbf{f}_i is updated at every time step.

Using FEM, forces are applied as boundary conditions

on elements in the reference mesh. Since the physician may insert the needle at any location, it is usually necessary to modify the reference mesh in real-time to ensure that element boundaries are present where the tip and friction forces must be applied. To apply the tip force, a node is maintained at the needle tip location during insertion. To apply the friction forces, a list of nodes along the needle shaft is maintained and these shaft nodes are constrained to only move horizontally along the needle shaft.

A. Cutting at the Needle Tip

Let point \mathbf{p} be the location of the needle tip in the reference mesh. At all times during needle insertion, a node c is constrained to be located at the needle tip point \mathbf{p} . Let i , j , and k be the nodes of a triangular element, as shown in Fig. 3. The needle tip at node $c=i$ is moving horizontally to the left as shown by the vector \mathbf{r}' in Fig. 3.b. This vector is linearly transformed to the reference mesh in Fig. 3.a and is denoted by \mathbf{r} . We assume that the x-component of \mathbf{r} is always points left. In the reference mesh, vector \mathbf{r} intersects the segment formed by nodes j and k at the point \mathbf{q} . Let f_c be the force applied by the needle at node c and let f_b represent the magnitude of the force required to cut a length b of tissue. When $f_c \geq f_b$, the tip of the needle moves a distance b along \mathbf{r} in the reference mesh to a new point $\mathbf{p}+\mathbf{br}$.

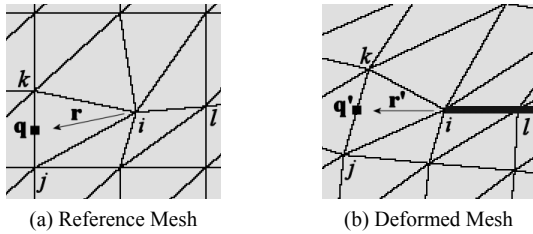


Fig. 3: The needle is in the interior of the mesh with needle tip node $c=i$ at point \mathbf{p} .

As \mathbf{p} approaches \mathbf{q} in Fig. 3, it is necessary to prevent a collision of node i with the segment (j,k) . Node l is the first node on the needle shaft behind the tip node. When the distance from node l to node i is more than twice the distance from node i to point \mathbf{q} , node i is added to the needle shaft: the x-component of node i is freed and the node is constrained to lie on the needle axis by fixing its y-component DOF. The closer of node j or k is moved to $\mathbf{p}+\mathbf{br}$ and is defined as the new tip node c . Key frames from a simulation using this type of mesh modification are shown in Fig. 4.

Moving nodes is not feasible in all cases. For a valid FEM computation, all elements must have strictly positive area. Consider the needle path shown in Fig. 5 and the corresponding mesh modifications. The tip node may move such that triangle (i,l,h) has negative area.

Negative area triangles are formed when the last shaft node l is either above or below both the previous shaft

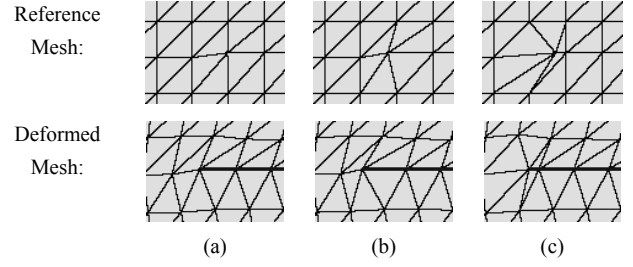


Fig. 4: The needle tip moves to the left in (a) through (c). The tip node is moved onto the shaft in (c) and the next tip node is selected.

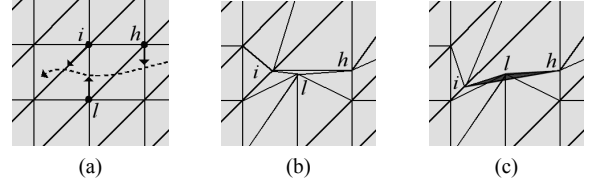


Fig. 5: A portion of a reference mesh with a needle path (the dotted line) is shown in (a) with tip node i and shaft nodes l and h . As the tip node i moves downward in (c), triangle (i,l,h) becomes degenerate.

node h and the tip node i . For this to occur, the y-component of \mathbf{r} must change sign twice over the span of just 2 element edges. Using a finer mesh prevents the formation of negative area triangles. Negative area triangles never occurred during the analysis in section VII, which used a 1250 element mesh and achieved real-time performance in interactive simulation mode.

B. Friction Along the Needle Shaft

Our approach to modeling static and kinetic friction between the needle shaft and the tissue is based on Baraff and Witkin [4], who modeled the friction between cloth and rigid objects. When the tangential velocity of a node along the needle shaft and the velocity of the needle are equal to within a small threshold v_s , then static friction is applied: the node is attached to the needle and moves at the same velocity. When the tangential force f_s required to attach the node to the needle exceeds the slip force parameter f_{s-max} , then the node is freed to slide along the needle shaft. When the tangential velocity exceeds a threshold parameter v_k , a dissipative force f_k is applied to the node. The dissipative force is proportional to the normal force, which we approximate as constant due to the needle's constant thickness and the uniformity of the tissue. To prevent oscillations after large time steps, $v_k > v_s$.

C. Membrane Puncture

The membrane surrounding the prostate is defined as a polygon whose vertices are points defined in the reference mesh. Let \mathbf{v}_k be the k 'th vertex of the prostate membrane. The containing mesh element e_k for each vertex \mathbf{v}_k is stored in memory. The location in the deformed mesh \mathbf{v}_k' of the k 'th membrane vertex can be found using the shape functions of e_k and the displacement of the element nodes in $O(1)$ time [25].

The force required to puncture the prostate membrane during needle insertion is greater than the force required to cut through soft tissue. Hence, when the segment $(\mathbf{p}, \mathbf{p}+b\mathbf{r})$ intersects an edge $(\mathbf{v}_k, \mathbf{v}_{k+1})$ of the membrane, a membrane cutting force f_m is used instead of the standard soft tissue cutting force f_b .

When any node \mathbf{j} of element e_k is moved during the simulation, it is necessary to update the containing element of \mathbf{v}_k . Since the point \mathbf{v}_k may only be inside an element containing node \mathbf{j} , the standard zero-winding rule for polygon inside-outside tests is applied to find the new containing element in $O(1)$ time.

D. Radioactive Seed Implantation

A seed is implanted at the location of the needle tip in the reference mesh. We assume that the seed does not move in the reference mesh after it is implanted. The location of the seed in the deformed mesh is computed using the same method as for vertices of a membrane described above.

E. Needle Retraction

During needle retraction, a tip node is not maintained since no cutting force is required. When the needle retracts past a node on the shaft, that node is removed from the shaft node list. Friction is applied on all the shaft nodes exactly as during insertion.

VI. SIMULATION IMPLEMENTATION

The simulator was implemented in C++ using OpenGL running on a 750MHz Pentium III PC with 128MB RAM. When executed in interactive simulation mode, a physician can guide the needle and implants seeds using a mouse. For a model with 1250 triangular elements the simulator responds at the rate of 24 frames per second, sufficient for visual feedback (but not fast enough for haptic control).

The visual feedback of the simulation is intended to mimic the experience of a physician performing brachytherapy. We believe this output can be useful for physician training [1]. A static pre-procedure ultrasound image of the prostate is used to manually generate the mesh, including the prostate membrane and the fixed boundary around the surrounding tissues. The simulation generates mesh deformations that simulate the tissue's response to the needle. A texture map of the original static ultrasound image is then deformed based on this mesh and is displayed to the user.

To set simulation parameters and validate our model, we compared the output of the simulation with ultrasound video taken from a real medical procedure. In June 2002, a needle insertion procedure was performed in the operating room at the UCSF Medical Center on a patient undergoing brachytherapy treatment for prostate cancer. The procedure was recorded using an ultrasound probe in

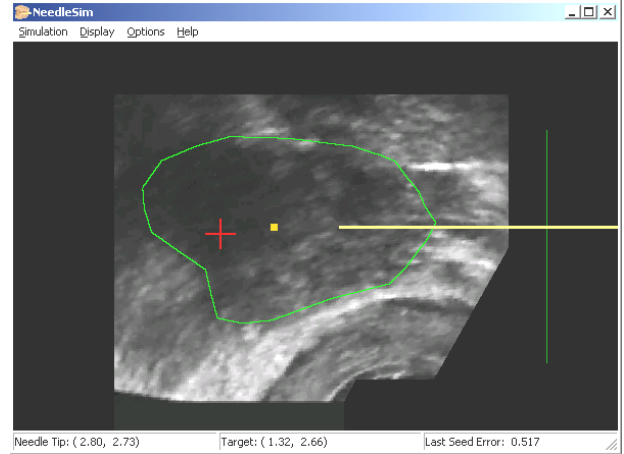


Fig. 6: The simulation user interface, which is based on an ultrasound image, is intended to mimic the experience of a physician performing brachytherapy. The physician interactively guides the needle using a mouse and implants seeds (small squares). Tissue deformations and seed locations are predicted and displayed. The implantation error is the distance between the seed and its target (cross) at equilibrium.

the sagittal plane, as shown in Fig. 2. The first frame of the ultrasound video was used to manually generate the mesh and texture map for the simulator. Unknown simulation parameters were set so that the simulation output closely matched the ultrasound video. Snapshots from the simulation output can be compared with frames from the ultrasound video, and are available at <http://alpha.ieor.berkeley.edu/ron/research>. Although it is difficult for non-specialists to identify gland boundaries in ultrasound, UCSF medical experts comparing the two image sequences judged them as remarkably similar. We plan to perform controlled experiments to further evaluate simulation accuracy across multiple patients.

VII. SENSITIVITY ANALYSIS

To measure sensitivity to simulation parameters, we simulate the implantation of a single seed and determine the seed placement error subject to changes in the parameters. For each numerical experiment, the target implant location is (x_t, y_t) in the reference mesh. Using our simulation, the needle is inserted at height y' to a depth x' in the world frame, the seed is implanted, the needle is fully retracted, and the tissue is allowed to settle. We compute (x_s, y_s) , the final location of the implanted seed. The seed placement error E is defined by the Euclidean distance from (x_s, y_s) to (x_t, y_t) . We use the target from Fig. 1 as a test case for a prostate with a 3.5cm width. Based on current medical practice, we set the default values of x' and y' to x_t and y_t , respectively. Other parameters are set so the simulation closely matches the ultrasound video in section VI, resulting in a default error of 0.65cm. We then independently test the sensitivity of the seed placement error to changes in physician-controlled and patient-specific parameters.

A. Sensitivity to Physician-Controlled Parameters

We first measure the sensitivity of the error to changes in the needle insertion depth and height. These are the parameters for which the physician has greatest control. As the needle moves left in Fig. 2, the target location is displaced to the left. Correcting for this by inserting the needle deeper than the target location depth decreases the error, as shown in Fig. 7. Modifying insertion height will generally increase error, as shown in Fig. 8.

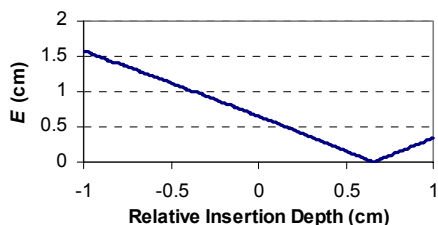


Fig. 7: Seed placement sensitivity to needle insertion depth. Error is in cm based on a 3.5cm prostate. Placement error can be reduced almost to zero by inserting the needle 0.65cm beyond the target depth; this compensates for tissue deformation during insertion.

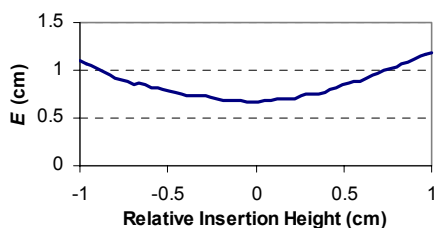


Fig. 8: Seed placement sensitivity to insertion height. Deviating the insertion height from the target height increases error.

The sharpness of a needle is inversely proportional to the amount of force required for the needle's tip to cut tissue. The needle sharpness parameter is scaled between 0 and 1, with higher values for sharper needles. Assuming constant tissue properties, sharper needles cut through the tissue more easily and hence cause smaller tissue deformations. As shown in Fig. 9, using a sharper needle decreases the error.

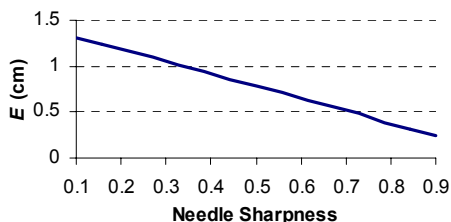


Fig. 9: Seed placement sensitivity to needle sharpness. A sharper needle decreases deformation and hence placement error.

We proportionately varied the coefficients of static and kinetic friction between the needle shaft and the tissue. Lower friction forces decreased the magnitude of tissue deformations and hence decreased error, as shown in Fig. 10.

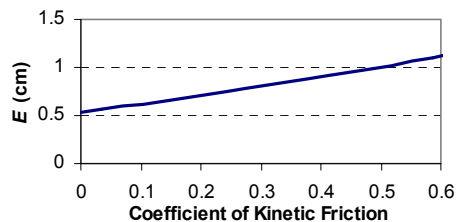


Fig. 10: Seed placement sensitivity to needle friction. A needle with low friction can reduce deformation during insertion and retraction.

Increasing needle insertion velocity decreases error, as shown in Fig. 11 due to damping and frictional effects. Greater needle velocity causes the nodes along the needle shaft to more quickly transition from static friction to the smaller kinetic friction, which results in smaller deformations. Unfortunately, needle velocity cannot be set arbitrarily high because physicians often need to stop and verify that the needle has not bent away from the desired path.

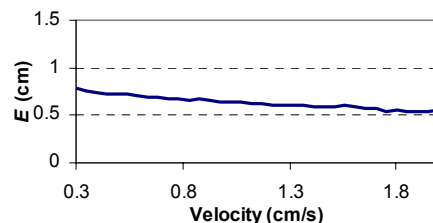


Fig. 11: Seed placement sensitivity to needle velocity. Increasing velocity decreases error because the effect of static friction is decreased.

B. Sensitivity to Patient-Specific Parameters

We varied the tissue's Young's modulus to test the sensitivity of the error to tissue stiffness. Although the physician must exert more force on the needle when the tissue is stiffer, the tissue deformations do not change significantly. The needle tip acts as a displacement constraint on the tissue, so greater tissue stiffness implies the needle exerts a proportionately greater force on the tissue. Our results show that the decreasing the stiffness moderately increases the error primarily because the cutting force becomes proportionately greater.

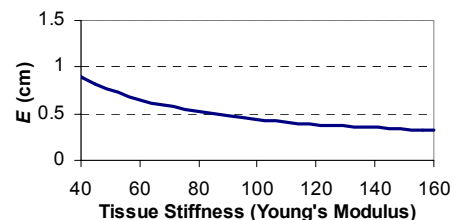


Fig. 12: Seed placement sensitivity to prostate tissue stiffness. Note that placement error is only moderately sensitive to tissue stiffness.

Soft human tissue is nearly incompressible with a Poisson ratio approaching 0.5 [11]. We varied this ratio between 0.4 and 0.499 in simulation but the error remained constant. The error is not sensitive to large changes in tissue compressibility.

VIII. CONCLUSIONS

This paper describes a new 2D model of needle insertion based on a dynamic FEM formulation and a reduced set of scalar parameters such as needle friction, sharpness, and velocity, where the mesh is updated to maintain element boundaries along the needle shaft and the effects of the needle tip and frictional forces are simulated. The computational complexity of the model grows linearly with the number of elements in the mesh and achieves 24 frames per second for 1250 triangular elements on a 750Mhz PC. The speed of the simulation is determined primarily by the scalability of the finite element method system solver. We described two solvers: an $O(d)$ explicit integration solver for interactive training and an $O(kd)$ implicit integration solver for higher accuracy planning, where the number of iterations k is bounded above by d . The value of d will not rise during a simulation because no new nodes are added, and it may in fact decrease as the y-axis DOF of some nodes are lost when they are constrained along the needle shaft.

Feedback from medical experts encouraged us to study the sensitivity of the model to physician-controlled planning parameters and patient-specific biological parameters. For a model to be useful for planning, it should be sensitive to physician-controlled parameters and relatively insensitive to patient-specific parameters, since the latter are difficult to estimate before the procedure.

The sensitivity analysis suggests that this is the case: inserting the needle deeper and/or using sharper needles with less surface friction can decrease seed placement error and that the variances of the biological parameters of global tissue stiffness and compressibility have only a minimal effect on seed placement error.

Our next step is to conduct controlled experiments to further evaluate simulation accuracy across multiple patients. We also plan to extend the model to 3D elements with non-homogeneous, nonlinear tissue properties and develop better models of membrane puncture.

IX. ACKNOWLEDGEMENTS

We thank Russ Taylor for bringing this problem to our attention and Tim Salcudean, Simon DiMaio, Allison Okamura, Dan Halperin, A. Frank van der Stappen, K. Gopalakrishnan, Dezhen Song, Han-Wen Nienhuys, Katja Langen, and Etienne Lessard for their valuable feedback.

X. REFERENCES

- [1] R. Alterovitz, J. Pouliot, R. Taschereau, I.C. Hsu, and K. Goldberg, "Simulating needle insertion and radioactive seed implantation for prostate brachytherapy," *Medicine Meets Virtual Reality 11*, J.D. Westwood et al. (Eds.), IOS Press, January 2003, pp. 19-25.
- [2] R. Alterovitz and K. Goldberg, "Comparing algorithms for soft tissue deformation: accuracy metrics and benchmarks," June 2002. Available: <http://alpha.ieor.berkeley.edu/ron/research/>
- [3] F. S. Azar, D. N. Metaxas, M. D. Schnall, "A deformable finite element model of the breast for predicting mechanical deformations under external perturbations," *Academic Radiology*, Vol. 8, No. 10, 2001.
- [4] D. Baraff and A. Witkin, "Large steps in cloth animation," *Computer Graphics Proceedings, SIGGRAPH*, 1998, pp. 43-54.
- [5] J. Brown, S. Sorkin, C. Bruyns, J.C. Latombe, K. Montgomery, M. Stephanides, "Real-time simulation of deformable objects: tools and applications," *Computer Animation*, Nov. 2001.
- [6] S. Cotin, H. Delingette, and N. Ayache, "Real-time elastic deformations of soft tissues for surgery simulation," *IEEE Trans. on Visualization and Computer Graphics*, Vol. 5, No. 1, 1999.
- [7] J. E. Dawson, T. Wu, T. Roy, J. Y. Gy, and H. Kim, "Dose effects of seeds placement deviations from pre-planned positions in ultrasound guided prostate implants," *Radiol. Oncol.* 32, 1994, pp. 268-270.
- [8] S. P. DiMaio and S. E. Salcudean, "Needle insertion modeling and simulation," in *Proc. of the IEEE Int. Conf. on Robotics and Automation*, May 2002, pp. 2098-2105.
- [9] L. A. Freitag and C. F. Ollivier-Gooch, "A cost/benefit analysis of simplicial mesh improvement techniques as measured by solution efficiency," *Int. Journal of Computational Geometry*, Vol 10, 2000.
- [10] S. F. Gibson and B. Mirtich, "A survey of deformable modeling in computer graphics," *MERL, TR-97-19*, 1997.
- [11] T. A. Krouskop, T. M. Wheeler, F. Kallel, B. S. Garria, and T. Hall, "Elastic moduli of breast and prostate tissues under compression," *Ultrasonic Imaging*, Vol. 20, 1998.
- [12] E. Lee, R. J. Gallagher, and M. Zaider, "Planning implants of radionuclides for the treatment of prostate cancer: an application of mixed integer programming," *Optima*, No. 61, March 1999.
- [13] H.W. Nienhuys and A. F. van der Stappen, "A surgery simulation supporting cuts and finite element deformation," in *Medical Image Computing and Computer-Assisted Intervention*, Oct. 2001, pp. 153-160.
- [14] G. Picinbono, H. Delingette, N. Ayache, "Nonlinear and anisotropic elastic soft tissue models for medical simulation," in *Proc. of the IEEE Int. Conf. on Robotics and Automation*, May 2001, pp. 1370-1375.
- [15] J. Pouliot, R. Taschereau, C. Coté, J. Roy, and D. Tremblay, "Dosimetric aspects of permanent radioactive implants for the treatment of prostate cancer," *Physics in Canada* 55(2), 1999, pp. 61-68.
- [16] J. Pouliot, D. Tremblay, J. Roy, and S. Filice, "Optimization of permanent 125I prostate implants using fast simulated annealing," *Int. J. Radiat. Onco. Biol. Phys.* 36(3), 1996, pp. 711-720.
- [17] C. Simone and A. M. Okamura, "Modeling of needle insertion forces for robot-assisted percutaneous therapy," in *Proc. of the IEEE Int. Conf. on Robotics and Automation*, May 2002, pp. 2085-2091.
- [18] R. Taschereau, J. Roy, and J. Pouliot, "Monte Carlo simulations of prostate implants to improve dosimetry and compare planning methods," *Med. Phys.* 26 (9), Sept. 1999.
- [19] D. Terzopolous, J. Platt, A. Barr, K. Fleischer, "Elastically deformable models," *Computer Graphics*, Vol. 21, No. 4, 1987.
- [20] K. Waters. A Muscle Model for Animating Three-Dimensional Facial Expression. *SIGGRAPH 87*, 1987.
- [21] W. L. Wood, "Some Transient and Coupled Problems - A State-of-the-Art Review," Chapter 8, *Numerical Methods in Transient and Coupled Problems*, R. W. Lewis et al., editors, 1987.
- [22] X. Wu, M.S. Downes, T. Goktekin, and F. Tendick, "Adaptive nonlinear finite elements for deformable body simulation using dynamic progressive meshes," *Eurographics 2001, Computer Graphics Forum*, Vol. 20, No. 3, Sept. 2001, pp. 349-358.
- [23] M. Zaider et al., "Treatment planning for prostate implants using magnetic-resonance spectroscopy imaging," *Int. J. Radiation Oncology Biol. Phys.*, Vol. 47, No. 4, 2000.
- [24] Y. Zhuang, "Real-time simulation of physically realistic global deformations," Ph.D. thesis, UC Berkeley, 2000.
- [25] O.C. Zienkiewicz and R.L. Taylor, *The Finite Element Method*, Fifth Edition, Butterworth-Heinemann, 2000.